



# Magnetoelastic coupling and phases in the skyrmion lattice magnet $\text{Gd}_2\text{PdSi}_3$ discovered by high-resolution dilatometry

S. Spachmann <sup>1,\*</sup>, A. Elghandour <sup>1</sup>, M. Frontzek<sup>2,3</sup>, W. Löser<sup>5</sup> and R. Klingeler<sup>1,4</sup>

<sup>1</sup>Kirchhoff Institute for Physics, Heidelberg University, Heidelberg, Germany

<sup>2</sup>Oak Ridge National Laboratory, Oak Ridge, Tennessee 37830, USA

<sup>3</sup>Institute of Solid State and Materials Physics, Dresden University of Technology, Dresden, Germany

<sup>4</sup>Centre for Advanced Materials (CAM), Heidelberg University, Heidelberg, Germany

<sup>5</sup>Leibniz Institute for Solid State and Materials Research (IFW), Dresden, Germany



(Received 18 March 2021; revised 20 April 2021; accepted 26 April 2021; published 21 May 2021)

We report detailed thermodynamic studies on high-quality single crystals of the centrosymmetric skyrmion-hosting intermetallic  $\text{Gd}_2\text{PdSi}_3$  by means of high-resolution capacitance dilatometry in fields up to 15 T which are complemented by specific heat and magnetization studies. Our dilatometric measurements show magnetoelastic effects associated with antiferromagnetic order at  $T_{N1} = 22.3$  K and  $T_{N2} = 19.7$  K, as well as strong field effects in an applied magnetic field of 15 T up to 200 K (150 K) for  $B \parallel c$  ( $B \parallel a^*$ , i.e.,  $B \perp c$ ). The data allow us to complete the magnetic phase diagram, including a feature at  $T^* \approx 13$  K below which an additional degree of freedom becomes relevant. The magnetic B vs T phase diagram for the  $a^*$  axis is also reported. Grüneisen analysis shows the onset of magnetic contributions around 60 K, i.e., well above  $T_{N1}$ . Uniaxial pressure dependencies of opposite signs,  $-1.3$  and  $0.3$  K/GPa, are extracted for the out-of-plane and in-plane directions at  $T_{N1}$ . For  $T^*$  we obtain  $\partial T^*/\partial p_c = 1.4$  K/GPa. In particular we elucidate thermodynamic properties of the recently discovered skyrmion lattice phase and show that it is strongly enhanced by uniaxial pressure.

DOI: [10.1103/PhysRevB.103.184424](https://doi.org/10.1103/PhysRevB.103.184424)

## I. INTRODUCTION

Ternary intermetallic compounds of the type  $R_2TX_3$  ( $R$  = rare earth,  $T$  = transition metal,  $X$  = element of main groups III to V) [1,2] have been investigated extensively over the past decades, due to their variety of intriguing electronic properties ranging from superconductivity [3], giant magnetoresistance (GMR) [4–6], ferromagnetism [7] and incommensurate spin structures [8,9], and phenomena related to Kondo physics and heavy fermions [10–12], to non-Fermi-liquid [10], and to spin-glass behavior [13–16]. This is particularly evident in the title material  $\text{Gd}_2\text{PdSi}_3$  where a skyrmion lattice phase featuring a giant topological Hall and Nernst effect was discovered recently [8,17,18].

Most members of the  $R_2\text{PdSi}_3$  family of ternary silicides crystallize in a highly symmetric  $\text{AlB}_2$ -derived hexagonal structure (space group  $P6/mmm$ ) with triangular lattice layers of  $R^{3+}$  magnetic sites sandwiching honeycomb nets of Pd and Si sites. While the Pd and Si ions were originally believed to be distributed statistically [19], an x-ray and neutron diffraction study by Tang *et al.* showed for  $\text{Ho}_2\text{PdSi}_3$  that these ions actually order into a superstructure along both in- and out-of-plane directions, while the overall centrosymmetry of the structure is retained [20]. This leads to two nonequivalent sites for the  $R^{3+}$  ions, which have been shown to affect the magnetism in an applied magnetic field for  $\text{Er}_2\text{PdSi}_3$  [21].

While no structural phase transition has been detected for  $R = \text{Gd}, \text{Tb}, \text{Dy}, \text{Ho}, \text{Er}, \text{and Tm}$ , most  $R_2\text{PdSi}_3$  compounds show long-range magnetic order at low temperatures [22–24].

These various ordering phenomena are driven by a delicate interplay of indirect exchange coupling mediated by the conduction electrons, i.e., the Rudermann-Kittel-Kasuya-Yosida (RKKY) interaction, spin-orbit coupling, and the influence of crystal field (CF) effects. The  $\text{Gd}^{3+}$  ions in  $\text{Gd}_2\text{PdSi}_3$ , however, with a half-filled  $4f$  shell, have vanishing orbital momentum ( $\mathbf{J} \approx \mathbf{S} = 7/2$ ) and are not influenced by crystal field effects. Magnetic order, therefore, arises from the RKKY interaction and dipole-dipole interactions.  $\text{Gd}_2\text{PdSi}_3$  exhibits two successive phase transitions around  $T_N = 21$  K [9] and was found to exhibit a skyrmion lattice (SkL) phase of Bloch-type skyrmions in low magnetic fields applied along the  $c$  axis [8]. A number of incommensurate spin structures both in zero field as well as in higher applied magnetic fields have been identified [9] and the phase diagram in fields up to 9 T has been established through resistance and magnetization measurements as well as resonant x-ray scattering [8,9,22,25]. Single crystal x-ray and neutron diffraction measurements yielded lattice parameters at 300 K (2 K) of  $a = 4.079$  Å (4.066 Å) and  $c = 4.098$  Å (4.091 Å), i.e.,  $\Delta a/a = 3.2 \times 10^{-3}$  and  $\Delta c/c = 1.7 \times 10^{-3}$  [20,26].

Except for these measurements of the lattice parameters, however, there is at present no study on magnetoelastic effects in  $\text{Gd}_2\text{PdSi}_3$ . Therefore, with a particular focus on the skyrmion lattice phase, we report detailed dilatometric studies of  $\text{Gd}_2\text{PdSi}_3$  in a wide range of temperatures and

\*sven.spachmann@kip.uni-heidelberg.de

magnetic fields. Our thermal expansion and magnetostriction data show pronounced magnetoelastic coupling and field effects extending up to temperatures of 150 K and above. Moreover, we uncover yet unreported phases and an anomaly in zero field which appears well below the Néel transitions at  $T_{N1} = 22.3(5)$  K and  $T_{N2} = 19.7(5)$  K, thereby evidencing competing interactions already in zero field. We update the magnetic phase diagram for the  $c$  axis (with  $B \parallel c$ ), present for the first time the phase diagram for the  $a^*$  axis (with  $B \parallel a^*$ ), and discuss in detail the thermodynamic properties for  $B \parallel c$ . Our results in particular elucidate the skyrmion lattice phase and we show that it is enhanced by uniaxial pressure.

## II. EXPERIMENTAL METHODS

Single crystals of  $\text{Gd}_2\text{PdSi}_3$  have been grown by the optical floating-zone method as reported in Refs. [27,28] and were previously studied by AC susceptibility, neutron diffraction [22], and angle-resolved photoemission spectroscopy [29]. The magnetization was studied in the temperature regime from 1.8 to 300 K in magnetic fields up to 7 T in a Magnetic Properties Measurement System (MPMS3, Quantum Design) and up to 14 T in a Physical Properties Measurement System (PPMS, Quantum Design) using the vibrating sample magnetometry option. Specific heat measurements were performed on a PPMS-14 using a relaxation method on single crystals of  $m = 20.79$  mg (2–300 K) and 13.49 mg (0.15–3 K). High-resolution dilatometry measurements were performed by means of a three-terminal high-resolution capacitance dilatometer in a home-built setup placed inside a variable temperature insert of an Oxford magnet system [30,31]. With this dilatometer, the relative length changes  $dL_i/L_i$  along the crystallographic  $c$  and  $a^*$  directions, respectively, were studied on an oriented cuboid-shaped single crystal of dimensions  $2.480 \times 1.300 \times 1.459$  mm<sup>3</sup>. Measurements were performed at temperatures between 2 and 300 K in magnetic fields up to 15 T, applied along the direction of the measured length changes, and the linear thermal expansion coefficients  $\alpha_i = 1/L_i \cdot dL_i(T)/dT$  were derived. In addition, the field-induced length changes  $dL_i(B_i)$  were measured at various fixed temperatures between 1.7 and 200 K in magnetic fields up to 15 T. The longitudinal magnetostriction coefficient  $\lambda_i = 1/L_i \cdot dL_i(B_i)/dB_i$  was derived from  $dL_i(B_i)$ .

## III. EXPERIMENTAL RESULTS

### A. Evolution of magnetic order at $B = 0$

Uniaxial thermal expansion and specific heat show pronounced anomalies around 20 K which are associated with the onset of long-range magnetic order (Fig. 1). Close inspection of the anomalies indicates the proximity of not only one but two phase transitions around  $T_N$ . While the anomaly at  $T_{N1} = 22.3(5)$  K is seen as a jump in  $\alpha_i$ , the anomaly at  $T_{N2} = 19.7(5)$  K [20.3(5) K for the  $a^*$  axis] is expressed as a peak. This observation confirms the results by Hirschberger *et al.* of two consecutive phase transitions in zero field [9]. Beyond these two known transitions, however, our data display a third anomaly indicative of a phase transition which has not been reported for single crystals of  $\text{Gd}_2\text{PdSi}_3$ . This anomaly, marked by  $T^* \approx 13$  K in the inset of Fig. 1(b), is visible as a

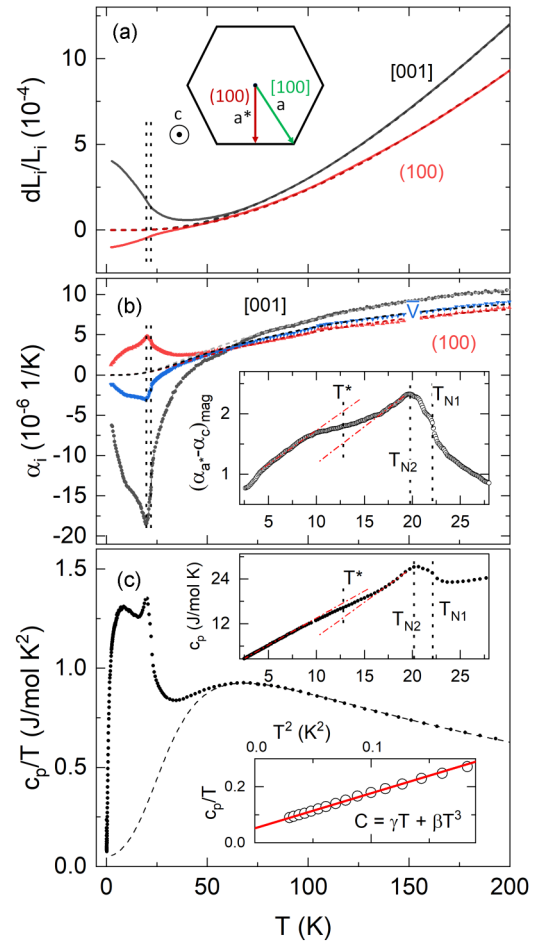


FIG. 1. (a) Relative length changes  $dL_i/L_i$  along the  $c$  and  $a^*$  crystallographic directions. Directions with respect to the Gd lattice are indicated in the inset. (b) Associated linear thermal expansion coefficients  $\alpha_i$  as well as the calculated  $1/3$  volume expansion  $\alpha_V$ . The inset displays the difference  $\alpha_{a^*} - \alpha_{c, \text{mag}}$  of the background-corrected thermal expansion coefficients  $\alpha_{i, \text{mag}} = \alpha_i - \alpha_{\text{ph}}$ . Vertical dashed lines indicate phase transitions and the dashed-dotted lines (inset) are a guide to the eye highlighting a feature around  $T^*$ . (c) Specific heat  $c_p/T$  (black markers). Inset: Low-temperature regime plotted as  $c_p/T$  vs  $T^2$ . The solid red line shows a fit with  $c_p = \gamma T + \beta T^3$ . Dashed curves in all graphs mark the nonmagnetic background as explained in the text.

broad jump for both directions in  $\alpha_i$  which extends between 10 and 15 K and is discussed in more detail below.

The specific heat data show the three observed features at  $T_{N1}$ ,  $T_{N2}$ , and  $T^*$ , too [Fig. 1(c)]. The shape of the anomalies in  $c_p$  is analogous to their shape in  $\alpha_{a^*}$ . At very low temperature below about 400 mK a quasilinear behavior of  $c_p/T$  vs  $T^2$  is found [see the inset of Fig. 1(c)], reminding one of similar observations in  $\text{Lu}_2\text{PdSi}_3$  and  $\text{Ce}_2\text{PdSi}_3$  [11,32]. In this temperature regime, the data are described well by a linear term and a cubic term, i.e.,  $c_p/T = \gamma + \beta T^2$ . The quasilinear term is described by an effective Sommerfeld coefficient,  $\gamma = 52(5)$  mJ/(mol K<sup>2</sup>). This parameter is in between the values obtained for  $\text{Lu}_2\text{PdSi}_3$  [6.9 mJ/(mol K<sup>2</sup>)] and  $\text{Ce}_2\text{PdSi}_3$  [108 mJ/(mol K<sup>2</sup>)], the latter being discussed as evidence of heavy-fermion behavior [11]. Whereas phonons can be

neglected in this temperature regime, the coefficient  $\beta = 1.25(3) \text{ J}/(\text{mol K}^4)$  is rather large and reflects the contribution of low-energy antiferromagnetic excitations.

The dashed lines in Fig. 1 show the phononic and electronic contributions to the relative length changes, thermal expansion coefficients, and specific heat. In order to obtain these contributions, the specific heat of the nonmagnetic analog  $\text{Lu}_2\text{PdSi}_3$  as reported by Cao *et al.* [32] was fitted by phononic Debye and Einstein terms, as well as an electronic term, according to

$$c_p^{\text{el,ph}} = \gamma T + n_D D\left(\frac{T}{\Theta_D}\right) + n_E E\left(\frac{T}{\Theta_E}\right), \quad (1)$$

where  $\gamma$  is the Sommerfeld coefficient,  $n_D$  and  $n_E$  are constants, and  $D(T/\Theta_D)$  and  $E(T/\Theta_E)$  are the Debye and Einstein functions with the Debye and Einstein temperatures  $\Theta_D$  and  $\Theta_E$ . The fit to the  $\text{Lu}_2\text{PdSi}_3$  specific heat data yields  $\Theta_D = 213 \text{ K}$  and  $\Theta_E = 454 \text{ K}$ , with  $n_D = 3.69$  and  $n_E = 1.98$ .  $\gamma$  was fixed to the value reported by Cao *et al.* of  $6.93 \text{ mJ}/\text{mol K}^2$  [32]. Compared to  $\Theta_D = 191 \text{ K}$  by Cao *et al.* [32], extracted from the low-temperature regime, our value is slightly larger.

Scaling the Debye and Einstein temperatures by the different masses of Lu and Gd we obtain a scaling factor [33] of  $\Theta_{D,\text{LPS}}/\Theta_{D,\text{GPS}} = 0.962$ . The specific heat and thermal expansion of  $\text{Gd}_2\text{PdSi}_3$  were thus fitted with fixed  $\Theta_D = 222 \text{ K} = \Theta_{D,\text{LPS}}/0.962$  and correspondingly  $\Theta_E = 471 \text{ K}$ . For the fit to the specific heat,  $\gamma = 52 \text{ mJ}/(\text{mol K}^2)$  was also fixed. For the thermal expansion the electronic contribution was negligibly small and therefore omitted; i.e., it was fitted by

$$\alpha^{\text{ph}} = n_D D\left(\frac{T}{\Theta_D}\right) + n_E E\left(\frac{T}{\Theta_E}\right) \quad (2)$$

with parameters  $n_D$  and  $n_E$ . The phononic contributions to  $dL_i/L_i$  in Fig. 1(a) were obtained by integrating the background obtained for the respective  $\alpha_i$ .

Subtracting the electronic and phononic backgrounds from the specific heat and thermal expansion coefficients yields their respective magnetic contributions which extend up to about 60 K. This agrees with the temperature regime where the magnetization exhibits a nonlinear field dependence up to 7 T (see Fig. S1 [34]). From  $c_{p,\text{mag}}/T$  the changes in magnetic entropy,  $S_{\text{mag}}$ , above 150 mK are calculated. We obtain a constant  $\Delta S_{\text{mag}}(T > 150 \text{ mK}) = 31.3 \text{ J}/(\text{mol K})$  above 60 K, which is 90% of the full expected magnetic entropy of  $2R \ln 8 = 34.6 \text{ J}/(\text{mol K})$ , where  $R$  is the universal gas constant.

Returning to the thermal expansion data, we see that the anomalies in the thermal expansion coefficients, at  $T_{N1}$  and  $T_{N2}$ , are of opposite sign for the  $c$  and  $a^*$  axes, indicating opposite pressure dependencies  $\partial T_{Ni}/\partial p_c < 0$  and  $\partial T_{Ni}/\partial p_{a^*} > 0$ . The volume thermal expansion also indicates a negative hydrostatic pressure dependence  $\partial T_{Ni}/\partial p < 0$  for both antiferromagnetic transitions.

The Grüneisen ratio of the thermal expansion coefficient and the specific heat is a valuable quantity to determine the relevant energy scales driving the system and to quantify its pressure dependencies. In the presence of one dominant energy scale,  $\epsilon$ , this ratio is independent of temperature and

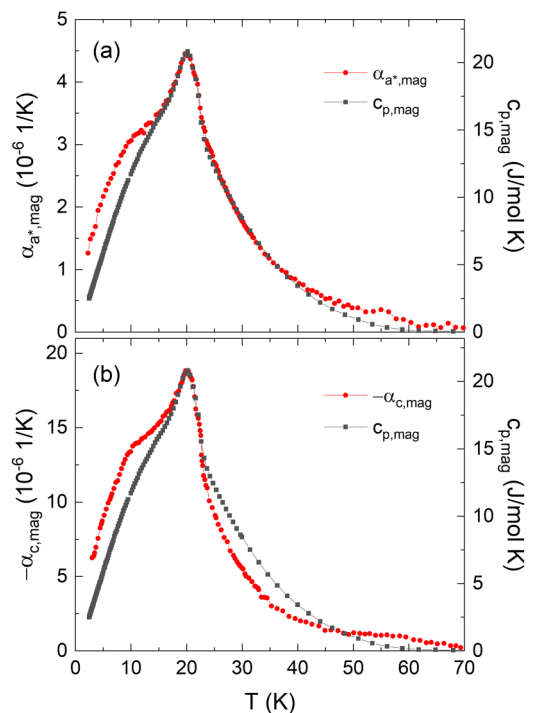


FIG. 2. Magnetic contributions to the thermal expansion coefficient (left axis) and specific heat (right axis) for (a) the  $a^*$  axis and (b) the  $c$  axis after subtracting phononic and electronic contributions as described in the text [37].

enables the determination of the pressure dependence of  $\epsilon$ , i.e., Refs. [35,36],

$$\Gamma_i = \frac{\alpha_i}{c_p} = \frac{1}{TV_m} \frac{\partial S/\partial p_i}{\partial S/\partial T} = \frac{1}{V_m} \frac{\partial \ln \epsilon}{\partial p_i}. \quad (3)$$

Here,  $V_m$  is the molar volume and the index  $i$  indicates a linear direction or the volume. At  $T_N$ , Eq. (3) converts to  $\Gamma = (T_N V_m)^{-1} (\partial T_N / \partial p)$ . Comparing the magnetic contributions  $\alpha_{i,\text{mag}}$  and  $c_{p,\text{mag}}$  hence allows one to identify temperature regimes where the Grüneisen relation implies only one dominant energy scale while appropriate scaling enables one to read off the respective parameter  $\Gamma_{i,\text{mag}}$ . As shown in Fig. 2, the overall behavior of  $\alpha_{i,\text{mag}}$  and  $c_{p,\text{mag}}$  is similar except for a distinct jump in  $\alpha_{i,\text{mag}}$  at  $\sim 12 \text{ K}$  which is much less pronounced in the magnetic specific heat. In both cases, magnetic contributions start to evolve around 60 K.

Despite the overall similar behavior, there are differences at higher temperatures, too. While the  $a^*$  axis shows a nearly perfect overlap between  $\alpha_{i,\text{mag}}$  and  $c_{p,\text{mag}}$  down to 14 K as shown in Fig. 2(a), we only observe a very good agreement around  $T_{N1}$  and  $T_{N2}$  for the  $c$  axis, in a range from 17 K to about 23 K. We also note that below  $\sim 14 \text{ K}$  our results indicate the failure of Grüneisen scaling rather than the presence of just a different scaling parameter.

Our data, however, clearly imply the presence of a single dominant energy scale at and around the magnetic ordering temperatures  $T_{N1}$  and  $T_{N2}$ . The obtained Grüneisen parameters amount to  $\Gamma_{c,\text{mag}} = -91(13) \times 10^{-8} \text{ mol}/\text{J}$  and  $\Gamma_{a^*,\text{mag}} = 22(3) \times 10^{-8} \text{ mol}/\text{J}$ . From these values, moderate pressure dependencies are derived; i.e., we obtain negative pressure

dependencies  $\partial T_{N1}/\partial p_c = -1.3(2)$  K/GPa and  $\partial T_{N2}/\partial p_c = -1.4(2)$  K/GPa for uniaxial pressure applied along the  $c$  axis. The uniaxial pressure dependencies for the  $a^*$  axis  $p \parallel a^*$  are positive and more than a factor of 4 smaller, i.e.,  $0.31(5)$  K/GPa for  $T_{N1}$  and  $0.34(5)$  K/GPa for  $T_{N2}$ .

While our data hence evidence that the ordering phenomena at  $T_{N1}$  and  $T_{N2}$  are governed by the same energy scale, an additional energy scale becomes relevant upon further cooling, around  $T^*$ , as proven by the failure of the Grüneisen scaling (cf. Fig. 2). Closer inspection of the associated anomalies implies not only a broad jump-like increase in the thermal expansion coefficients but also a less pronounced anomaly in  $c_p$  which is visible much more clearly in the  $c_p/T$  data in Fig. 1(c). In an attempt to deduce the anomaly size associated with the respective features we obtain  $\Delta c_p^* \approx 2.7(5)$  J/(mol K),  $\Delta \alpha_{a^*}^* \approx 1.8 \times 10^{-6}/\text{K}$ ,  $\Delta \alpha_c^* \approx 4.1(6) \times 10^{-6}/\text{K}$ , and  $\Delta \alpha_{a^*}^* \approx -1.0(3) \times 10^{-6}/\text{K}$ . The changes in magnetization around  $T^*$  are very small for both axes and could not be seen in the isothermal magnetization  $M(B)$ . However, temperature sweeps of the magnetization in the static field evidence a jump in  $\partial \chi/\partial T$ , which is visible for  $B \geq 0.2$  T (0.25 T) for  $B \parallel c$  ( $B \parallel a^*$ ) (see Supplemental Material, Fig. S10(a) [34]). At 0.2 T the jump height  $\Delta(\partial M/\partial T)$  amounts to  $5.6(1.4) \times 10^{-3} \mu_B/(\text{f.u. K})$ . Further values are listed in Table S7 [34].

### B. Thermal expansion at $B \neq 0$ and magnetostriction

The effect of high magnetic fields on the thermal expansion and specific heat is shown in Fig. 3. A number of observations can be made.

(i) The sharp features indicating phase transitions are absent at  $B = 15$  T.

(ii) Significant entropy is shifted to higher temperatures, and at  $B = 15$  T, significant field effects are visible at least up to 150 K in all shown quantities, in particular for  $\alpha_c$  even up to about 200 K.

(iii) Magnetostriction from 0 to 15 T is positive (negative) for the  $c$  axis ( $a^*$  axis).

(iv) The temperature region of negative thermal expansion of the  $c$  axis extends up to about 65 K at 15 T, compared to 38 K in zero field.

Note that the magnetostriction data fully agree with the thermal expansion data at  $B \neq 0$  T as shown by the (green) vertical lines in the inset of Fig. 3.

Magnetostriction data at  $T \approx 2$  K shown in Figs. 4(a) and 4(d) further confirm strong magnetoelastic coupling and in addition clearly show the field-induced phase transitions. For comparison the isothermal magnetic susceptibility  $\chi(B) = \partial M(B)/\partial B$  is also presented on the same field scale for both directions [Figs. 4(b) and 4(c)]. Considering the data for  $B \parallel c$ , four anomalies can be identified [Fig. 4(a)]: Up to 3.5 T, there are two sharp peaks in  $\lambda_c$  signaling jumps in  $dL_c(B)$  with only small field-hysteresis, followed by a broad peak with a large hysteresis of  $\sim 0.8$  T. The size of the anomalies for up- and down-sweep differs strongly. All three anomalies indicate discontinuous phase transitions. Corresponding anomalies and hystereses are also visible in the magnetic susceptibility. In addition, there is a broad downward jump in  $\lambda_c$  at around 9 T, above which magnetostriction becomes virtually zero which

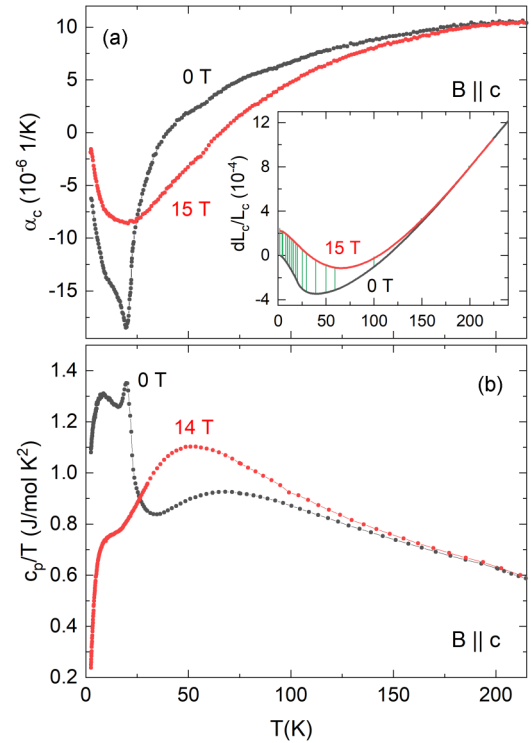


FIG. 3. The effect of high fields on (a) the thermal expansion coefficient ( $B = 15$  T) and (b) the specific heat  $c_p/T$  ( $B = 14$  T) as compared to zero-field measurements. The inset in panel (a) shows the relative length changes. Vertical green bars indicate magnetostriction data from 0 to 15 T at several temperatures.

is also reflected by small  $\chi$ , i.e., rather full alignment of magnetic moments in the field [please note the logarithmic scale in Figs. 4(b) and 4(c)]. The overall region where hysteresis is visible extends from about 6 T down to the lowest fields [see the inset in Fig. 4(a)], but no remanent magnetostriction is visible which would indicate irreversible changes in the sample, e.g., through domain effects. Four features are also visible in  $\lambda_{a^*}$  for  $B \parallel a^*$  [Fig. 4(d)]. These anomalies are smaller in magnitude, much broader, and less well-defined than for the  $c$  axis. Similar to the findings for  $\lambda_c(B \parallel c)$ , there is a jump at higher fields, at about 7.3 T, but here of opposite sign. Again, it signals a continuous transition to the saturated phase of vanishing magnetostriction. In contrast to  $B \parallel c$ , the magnetostriction measurements  $dL_{a^*}(B \parallel a^*)$  feature pronounced remanent magnetostriction below 5 K, i.e., nonzero overall length changes after sweeping the field from 0 to 15 T and back to 0 T. At 1.8 K, this amounts to  $(\Delta L/L)_{\text{rem}} = 1.4 \times 10^{-5}$ . We attribute this observation to the irreversible effects of structural or magnetic domains as seen, e.g., in CoCl<sub>2</sub> [38], NiCl<sub>2</sub> [39], and NiTiO<sub>3</sub> [40]. Such irreversible domain effects seem to be absent in the measurements along the  $c$  axis. The transition between a multidomain and single-domain state may thus be fully reversible for  $B \parallel c$ . We conclude that hysteresis found for  $B \parallel a^*$  below 3.5 T is due to both the discontinuous nature of the phase transitions and the domain effects.

Both data sets, hence, imply a series of four phase transitions in the magnetic field, at  $T \approx 2$  K, which is further corroborated by magnetization studies (also see Fig. S7

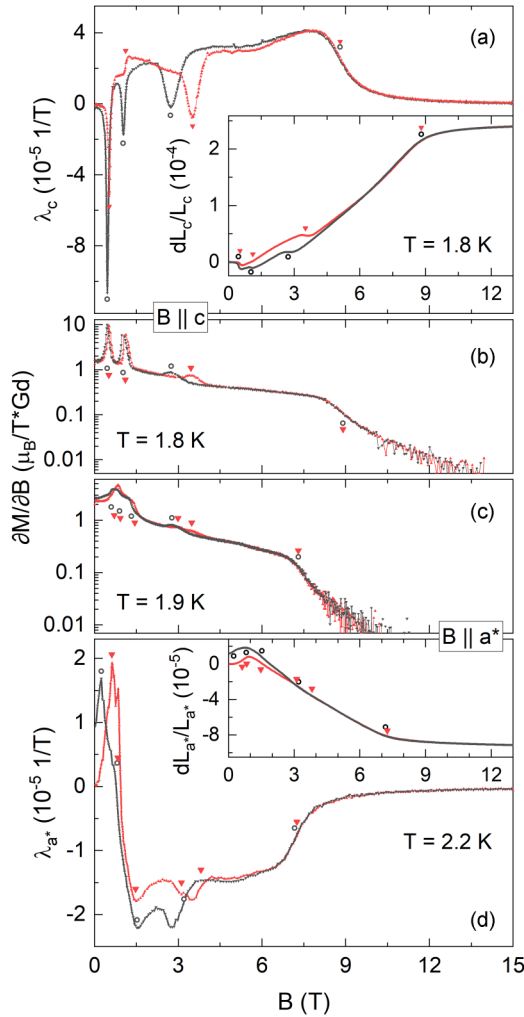


FIG. 4. Magnetostriction coefficients  $\lambda_i$  ( $i = c$  and  $a^*$ ) and isothermal magnetic susceptibility,  $\partial M/\partial B$ , at temperatures around 2 K, for  $B \parallel c$  [panels (a) and (b)] and  $B \parallel a^*$  [panels (c) and (d)]. Note the logarithmic scale in panels (b) and (c). Insets in panels (a) and (d) show the relative length changes  $dL_i(B)/L_i$ . Triangles and empty circles mark anomalies in panels (a)–(d). Red markers and lines represent up-sweeps; black ones represent down-sweeps.

[34]) and agrees with the recently published phase diagram for  $B \parallel c$  [9]. Following the notations in Refs. [8,9] for the phases appearing for  $B \parallel c$ , we label the respective phases as IC-1, A, IC-2, DP, and field-induced ferromagnetic (fiFM) phase, with IC-1/IC-2 being characterized by incommensurate spin configurations, A by the formation of a skyrmion lattice (SkL), and DP by the depinning of the direction of magnetic moments (see also the phase diagram in Fig. 6). We note, however, that while the magnetostriction data evidence field-driven structural changes, domain effects may obscure the actual phase transitions up to the field and temperature regions at which a single domain state is achieved. In particular, broad peaks in the magnetostriction coefficients as seen in  $\lambda_{a^*}$  (Figs. 4(b), S4(e), and S4(f) [34]) do not necessarily indicate the actual phase boundaries, but the peak positions may differ from those found in the magnetization studies, as shown by a phenomenological model by Kalita

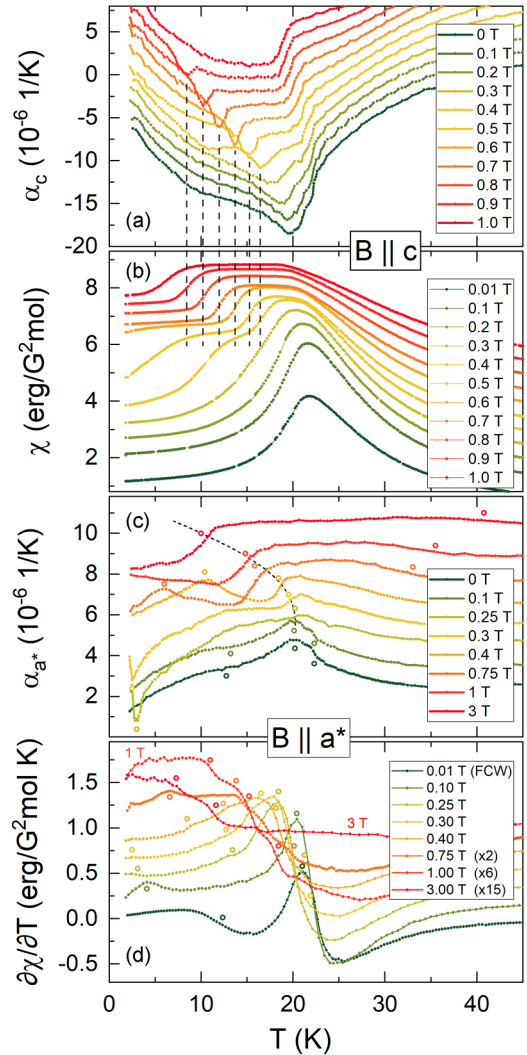


FIG. 5. Thermal expansion coefficients (a, c) and static magnetic susceptibility  $\chi = M/B$  (b), and its derivative  $\partial\chi/\partial T$  (d), for (a, b)  $B \parallel c$  and (c, d)  $B \parallel a^*$ . Curves are offset vertically by (a)  $1.6 \times 10^{-6}/\text{K}$ , (b)  $0.5 \text{ erg}/(\text{G}^2 \text{ mol})$ , (c)  $1 \times 10^{-6}/\text{K}$ , and (d)  $0.2 \text{ erg}/(\text{G}^2 \text{ mol K})$ , for better visibility. 0.75 to 3 T data in panel (d) are multiplied by a constant as indicated in the legend and 3 T data are offset by  $1.5 \text{ erg}/(\text{G}^2 \text{ mol K})$  instead of  $1.4 \text{ erg}/(\text{G}^2 \text{ mol K})$ . “FCW” indicates a field-cooled-warming measurement [41]. Empty circles mark temperature positions of the anomalies as extracted for the phase diagram.

*et al.* [38]. Therefore, for the further thermodynamic analysis of the phase boundaries as well as the construction of the phase diagram, for  $B \parallel a^*$  we only consider anomalies in the magnetostriction which can directly be linked to anomalies in isothermal magnetization.

In order to obtain the phase boundaries, we have performed thorough magnetostriction and isothermal magnetization studies at various fixed temperatures as well as corresponding temperature sweeps at fixed magnetic field (see Figs. S4, S5, S7 [34]) [42]. This is demonstrated in Fig. 5, where the thermal expansion coefficients in low fields up to 3 T and the corresponding magnetization data are presented. For  $B \parallel c$  [Figs. 5(a) and 5(b)], the evolution of two different phase

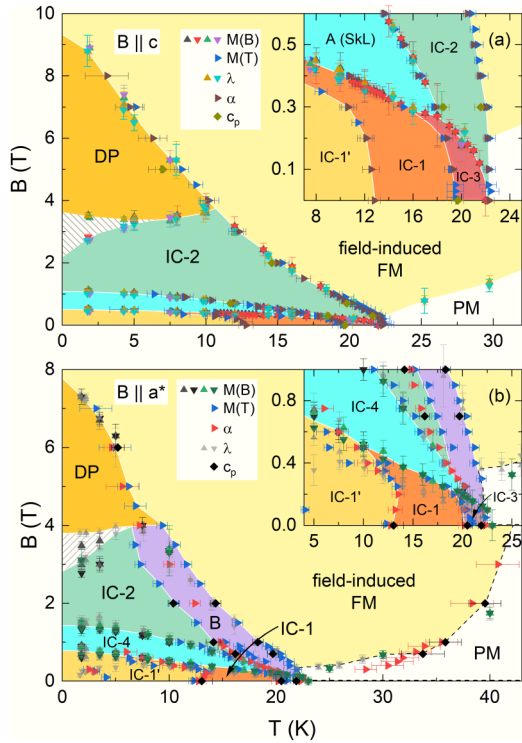


FIG. 6. Phase diagrams for (a)  $B \parallel c$  and (b)  $B \parallel a^*$  constructed from different experimental techniques as indicated in the legends. The shaded areas show two strong hysteresis regimes. The abbreviations for the phases are the following: paramagnetic, PM; incommensurate magnetic orders, IC- $x$ ; antiferromagnetic, A and B; antiferromagnetic skyrmion lattice, SkL; and depinned phase, DP.

boundaries can be traced straightforwardly. Specifically, applying small fields yields a suppression of  $T_{N2}$  while the jump at  $T_{N1}$  becomes more distinguished. In an increasing field,  $T_{N1}$  is also suppressed to a lower temperature, but to a smaller extent [Fig. 5(a)]. Above 0.3 T, the peak assigned to  $T_{N2}$  at zero field changes its shape, signaling the transition from the previously reported skyrmion lattice A phase to the IC-2 phase. It is associated with a jump,  $\Delta\chi_c^A$ , in the static susceptibility from one  $T$ -independent value to another [Fig. 5(b)]. At 0.4 T, a second feature corresponding to the transition from the A phase to the IC-1 phase is visible in both  $\alpha_c$  and  $\chi_c$ , while above 0.9 T (1 T for  $\chi_c$ ) all features below  $T_{N1}$  are gone. Quantitatively,  $\Delta\chi_c^A$  gradually decreases from  $0.91 \mu_B/\text{Gd}^{3+}$  at 0.9 T and 8.6 K to  $0.36 \mu_B/\text{Gd}^{3+}$  at 0.4 T and 16.4 K. The pronounced jump in  $\alpha_c$  at  $T_{N1}$  corresponds to a kink in the static susceptibility, i.e., a jump in its derivative (see Supplemental Material, Fig. S7 [34]).

As mentioned before, anomalies seen for measurements along the  $a^*$  axis are in general much weaker and less well-defined than those for the  $c$  axis. Furthermore, the evolution of anomalies in the thermal expansion and the static susceptibility along the  $a^*$  axis is even more complex than for  $B \parallel c$  [Figs. 5(c) and 5(d)]. In zero field, the anomaly at  $T^*$  is also visible (see Fig. 1, as well as Supplemental Material, Fig. S10(d) [34]) and can be traced up to 0.4 T in  $\partial\chi/\partial T$ . Also, a jump in  $\alpha_{a^*}$  evolving from  $T_{N1}$  can be followed to lower temperatures for increasing fields, corresponding to a

jump in  $\partial\chi/\partial T$ . Above 0.6 T this jump splits into two jumps, uncovering an additional phase between the IC-2 and the fiFM phases, while we only see one broad jump in  $\alpha_{a^*}$ .

#### IV. DISCUSSION

From our detailed dilatometric and thermodynamic data we construct the phase diagrams for the  $c$  and  $a^*$  axes in Fig. 6. While the general features for  $B \parallel c$  confirm previous results [8,9,25], our data evidence two phases in zero field which were previously unknown.

(i) Our isothermal magnetization data between 19 and 22 K (Supplemental Material, Fig. S7 [34]) clearly indicate that the IC-2 phase does not extend to zero field, but there is a separate pocket closed off by a phase boundary extending from the edge of the A(SkL) phase to  $T_{N1} = 22.3$  K. We label this phase IC-3, since incommensurate spin structures were previously reported for this temperature regime [8].

(ii) Furthermore, the phase boundary at  $T^*$  splits the IC-1 phase into IC-1 and IC-1' [Fig. 1(b) inset].

The yet unreported phase diagram for  $B \parallel a^*$  in general shows a similar behavior, with the critical fields of the IC-1' and IC-4 phases at the lowest temperatures assuming higher values than IC-1' and the A phase for the  $c$  axis. The IC-4 phase appearing for  $B \parallel a^*$  [see Fig. 6(b)] reminds one of the A(SkL) phase for  $B \parallel c$ ; however, it was shown previously by angle-dependent resistivity measurements in the  $a^*$ - $c$  plane at 2 K that it does not connect to the A(SkL) phase [43]. The magnetic structure of this phase needs to be clarified by diffraction studies. One major difference between the phase diagrams is seen for  $B \parallel a^*$ , where the IC-2 phase is not directly adjacent to the field-induced FM phase, but there is an additional phase (labeled B) in between [see Figs. 5(c) and 5(d)]. The B phase is bordered by two jumps both in  $c_p$  as well as in  $\partial\chi/\partial T$ .

From the anomalies in the thermal expansion, specific heat, and magnetization at the phase boundaries we calculated the uniaxial pressure and field dependence of the critical temperatures and critical fields, as well as the entropy changes at the phase boundaries for the  $c$  axis (with  $B \parallel c$ ). Considering  $T^*(B)$  marking a continuous phase transition, the associated jumps in the specific heat ( $\Delta c_p$ ), the magnetic susceptibility [ $\Delta(\partial M/\partial B)$ ], and the thermal expansion coefficient ( $\Delta\alpha$ ) are connected with the magnetic field and pressure dependencies of  $T^*$  by the Ehrenfest-type relations (see e.g. Refs. [44,45]):

$$\left(\frac{\partial T^*}{\partial B_i}\right)\Big|_p = -T^* \frac{\Delta\left(\frac{\partial M_i}{\partial T}\right)\Big|_B}{\Delta c_{p,B}} \quad (4)$$

and

$$\left(\frac{\partial T^*}{\partial p_i}\right)\Big|_B = T^* V_m \frac{\Delta\alpha_i}{\Delta c_p}. \quad (5)$$

Using the molar volume  $V_m = 7.06 \times 10^{-5} \text{ m}^3/\text{mol}$  (see Ref. [22]) as well as the anomaly values presented above and in Table S7—for their extraction from the experimental data see the Supplemental Material, Fig. S10 [34]—we obtain a moderate uniaxial pressure dependence of  $\partial T^*/\partial p_c = -1.4(3) \text{ K/GPa}$ . In a field of 0.2 T, the field dependence is very small and amounts to only  $\partial T^*/\partial B_c = -37(13) \text{ mK/T}$ .

At 0.3 T,  $\partial T^*/\partial B_c$  rises to  $-0.28(18)$  K/T. These results demonstrate that the IC-1 phase is stabilized both under pressure and applied field at the expense of the IC-1' phase. Also, from these values we can calculate the expected jump in  $\partial M/\partial B$  ( $\Delta\chi$ ) at  $T^*(B)$  via

$$\left(\frac{\partial T^*}{\partial B}\right)\Big|_p = -\frac{\Delta\left(\frac{\partial M}{\partial B}\right)\Big|_{p,T}}{\Delta\left(\frac{\partial M}{\partial T}\right)\Big|_{p,B}}. \quad (6)$$

At 0.2 T this yields  $\Delta\chi = -2 \times 10^{-4} \mu_B/(\text{f.u. T})$ , which is well below the resolution limit of our experiment, explaining why our isothermal magnetization studies do not show anomalies at  $T^*$  (see Supplemental Material, Fig. S10 [34]). Note that in an early report on  $\text{Gd}_2\text{PdSi}_3$  by Mallik *et al.* [52], the authors detected a jump in the effective local field  $|B_{\text{eff}}|$  at 15 K by Mössbauer spectroscopy and attributed it to a lower ordering temperature of one of the two Gd sites in  $\text{Gd}_2\text{PdSi}_3$ . This transition was not detected in any of the later reports on single crystalline samples, but our results presented in this work clearly confirm its presence.

The phase boundaries between the A(SkL), IC-2, and DP phases are of a discontinuous nature, exhibiting jumps  $\Delta L_i/L_i$  in the length changes and  $\Delta M$  in the magnetization (i.e.,  $\Delta m$  in magnetic moment). Therefore, the Clapeyron equations [44],

$$\left(\frac{\partial T_c}{\partial p_i}\right)\Big|_B = V_m \frac{\Delta L_i/L_i}{\Delta S}, \quad (7)$$

$$\left(\frac{\partial T_c}{\partial B_i}\right)\Big|_p = -\frac{\Delta m_i}{\Delta S} = -\frac{\Delta(M_i V)}{\Delta S}, \quad (8)$$

$$\left(\frac{\partial B_c}{\partial p_i}\right)\Big|_T = V_m \frac{\Delta L_i/L_i}{\Delta m_i}, \quad (9)$$

apply for the pressure and field dependence of the respective critical temperatures  $T_c$  and critical fields  $B_c$ . Hence, the observed slopes  $\partial T_c/\partial B$  (see Tables S1–S4 [34]) and the jumps  $\Delta M$  allow us to obtain the associated entropy changes  $\Delta S$ .

For the transition from the incommensurate IC-1' phase to the skyrmion lattice A phase, a jump of  $\Delta M = 0.99(10) \mu_B/\text{Gd}$  accompanies the  $c$  axis contraction of  $\Delta L_c/L_c = -10.8(1.1) \times 10^{-6}$  at 4.3 K. Applying the abovementioned thermodynamic relations yields small entropy changes on the order of  $\Delta S_{\text{calc}} = 125(13)$  mJ/mol K and a negative uniaxial pressure dependence of  $\partial T_c/\partial p_i = -6.1(9)$  K/GPa. At higher temperatures these values decrease down to 110(11) mJ/mol K and  $-1.5(2)$  K/GPa at 16 K (see Table S1 [34]). At the transition from the skyrmion lattice A phase to the IC-2 phase the  $c$  axis also contracts, but these contractions are much smaller ( $\Delta L_c/L_c = -2.4(3) \times 10^{-6}$  at 4.3 K) while the jumps in magnetization again roughly correspond to one Bohr magneton per Gd ion [ $\Delta M = 1.01(11) \mu_B/\text{Gd}$  at 4.3 K]. Accordingly, this phase boundary shows a much smaller pressure dependence, i.e.,  $\partial T_c/\partial p_i = -0.47(7)$  K/GPa at 4.3 K (see Table S2 [34]). At the same time, the steeper slope of the phase boundary  $B_c(T)$  implies larger changes in entropy of 360(40) mJ/mol K at 4.3 K which increases to almost 600(60) mJ/mol K at 16 K. We note that the analysis of anomalies from temperature instead of field sweeps confirms these values (Table S3 [34]). Looking at higher fields, the slope of the phase boundary from IC-2 to the depinned phase (DP) is very

small, changing from a small negative slope below 6 K to a small positive slope above. Considering the measured anomalies  $\Delta M = 0.08(4) \mu_B/\text{Gd}$  at 4.3 K, this yields negligible associated entropy changes (Table S4 [34]). In contrast, there are pronounced lattice effects ( $\Delta L_c/L_c = -17(2) \times 10^{-6}$  at 1.77 K) yielding a very large pressure dependence for the phase boundary IC-2  $\rightarrow$  DP.

The results of the thermodynamic analyses are shown in Table I as well as in Tables S1 to S4 in the Supplemental Material [34]. In particular, our analysis evidences pronounced negative uniaxial pressure dependencies for all three phase transitions between IC-1/IC-1', A(SkL), IC-2, and DP at low temperatures. This implies that the IC-1'/IC-1, A(SkL), and IC-2 phases are all destabilized by pressure along the  $c$  axis with respect to the higher temperature phases, i.e., the field-induced FM phase—and the paramagnetic phase at low fields—is stabilized.

In particular, our data for  $B \parallel c$  provide further information on the skyrmion phase. Both the onset of the SkL phase from the incommensurate magnetic order IC-1/IC-1' and its transition into the incommensurate IC-2 phase are discontinuous in nature. In both cases, transitions are associated with the increase of magnetization by about  $1 \mu_B/\text{Gd}$ . Rather flat phase boundaries in the magnetic phase diagram are indicative of comparably small entropy changes. Our quantitative analysis evidences that the evolution of the SkL phase, depending on the temperature, yields an entropy gain of  $\Delta S \approx 100\text{--}150$  mJ/(mol K) while the entropy jumps at the transition out of the skyrmion phase by  $300\text{--}600$  mJ/(mol K). These values are by far larger than those for the chiral magnet MnSi where latent heat at the phase boundaries only amounts to a few mJ/(mol K) [46]. Uniaxial pressure along the  $c$  axis significantly enhances the SkL phase as seen by the uniaxial pressure dependencies of the transition temperatures. Specifically, at 4 K there is a rapid decrease of the IC-1/IC-1'  $\rightarrow$  A(SkL) transition temperature  $\partial T_{\text{in}}/\partial p_c \approx -6$  K/GPa, leading to an expansion of the A(SkL) phase towards lower temperatures under pressure. At the same time the temperature of the A(SkL)  $\rightarrow$  IC-2 transition, i.e., exiting the SkL phase towards higher temperatures, changes by only  $\partial T_{\text{out}}/\partial p_c \approx -0.5$  K/GPa (see Tables I and II). Enhancement of skyrmion lattice phases under pressure is also observed in other materials. In the insulating skyrmion system  $\text{Cu}_2\text{OSeO}_3$ , Levatić *et al.* report a dramatic enhancement of the skyrmion pocket under pressure by about 8 K at 0.6 GPa [47]. While in  $\text{Gd}_2\text{PdSi}_3$  the SkL phase appears at lower temperatures, our results ( $\partial T_{\text{in}}/\partial p_c - \partial T_{\text{out}}/\partial p_c$ ) imply about half of this effect. We also note findings similar to the ones reported at hand in the chiral magnet MnSi [48,49] where uniaxial pressure along [001] yields a rapid decrease of the onset temperature of the skyrmion phase while the high-temperature phase boundary shows a much smaller pressure dependence [50]. Recent theoretical studies by Hayami *et al.* investigated the influence of single-ion anisotropy on the formation and stability of the skyrmion lattice phase. They show that easy-axis anisotropies stabilize magnetic-field-induced skyrmion crystals in frustrated magnets [51] and easy-axis (easy-plane) anisotropy substantially increases (decreases) the stable field-range for a Skyrmion lattice. These findings suggest that the pressure dependencies stabilizing the skyrmion lattice phase

TABLE I. Relevant quantities and anomaly sizes at the phase boundaries of the skyrmion lattice phase, at  $T = 4.3$  K, and in magnetic fields  $B \parallel c$  which have been either directly extracted from the experimental data or were obtained by using thermodynamic relations as given in the text.

Transition	$T$ (K)	$B_c$ (T)	$\Delta L/L$ ( $10^{-6}$ )	$\Delta m$ ( $\mu_B/\text{Gd}$ )	$\partial B_c/\partial T$ (T/K)	$\Delta S$ (mJ/mol K)	$\partial T_c/\partial p_i$ (K/GPa)	$\partial B_c/\partial p_i$ (mT/GPa)
IC-1 $\rightarrow$ A(SkL)	$4.3 \pm 0.1$	$0.49 \pm 0.02$	$-10.8 \pm 1.1$	$1.0 \pm 0.1$	$-0.01$	$125 \pm 13$	$-6.1 \pm 0.9$	$-50 \pm 50$
A(SkL) $\rightarrow$ IC-2	$4.3 \pm 0.1$	$1.04 \pm 0.03$	$-2.4 \pm 0.3$	$1.0 \pm 0.1$	$-0.03$	$360 \pm 40$	$-0.47 \pm 0.07$	$-15 \pm 2$

in  $\text{Gd}_2\text{PdSi}_3$  may originate from small distortions in the local environment of Gd, leading to an increase of the weak magnetic anisotropy of the Gd moments.

The transition from the depinned phase to the field-induced ferromagnetic phase is of a continuous type. It exhibits a jump in the magnetostriction coefficient  $\Delta\lambda = -4.7(5) \times 10^{-5}/T$  (at 1.77 K) and in the derivative of the magnetization  $\Delta(\partial M/\partial B) = -0.159(16) \mu_B/(\text{T Gd})$  ( $T = 1.9$  K). Using an Ehrenfest relation, the uniaxial pressure dependence of the critical field can be expressed as  $\partial B_c/\partial p_i = \Delta\lambda/\Delta(\partial M/\partial B)$ , which yields  $\partial B_c/\partial p_c = 1.9(5)$  T/GPa at 1.77 K, i.e., the depinned phase is stabilized under uniaxial pressure  $p_c$ . Similarly, using the anomaly values listed in Table S5 [34], we find uniaxial pressure dependencies of the critical field between  $-0.65(16)$  T/GPa (10 K) and  $-0.50(8)$  T/GPa (14 K) at the continuous transition IC-2 to f1FM.

While  $\text{Gd}_2\text{PdSi}_3$  shows only moderate frustration, magnetic entropy and length changes are observed up to about  $2.7 T_{N1}$  (60 K), thereby implying the evolution of short-range magnetic order in this temperature regime. Effects of fluctuations above  $T_N$  in  $\text{Gd}_2\text{PdSi}_3$  were observed before in resistivity measurements. Measurements on polycrystalline samples show a well-defined minimum around 45 K [52] which was also confirmed in single crystals [17]. A theoretical explanation of this behavior based on the RKKY interaction in combination with frustration was given by Wang *et al.* [53]. Grüneisen scaling suggests that these precursor fluctuations are of the IC-1/IC-3 type. Both ordering phenomena are driven by the same dominating energy scale which differs from the one driving IC-1'. As expected for a  $\text{Gd}^{3+}$  system, magnetoelastic coupling is moderate. It is, hence, somehow surprising that magnetostriction is large at high temperatures and displays pronounced effects up to 200 K. In addition, despite a linear field dependence of the magnetization, magnetostriction does not follow a  $B^2$  law below 200 K (see Fig. S6 [34]) as would be expected from the relation  $dL_i/L_i =$

$-1/2V\partial\chi_i/\partial p_i B^2$  in the paramagnetic regime [54]. Tentatively, magnetostriction above 100 K implies negative uniaxial pressure dependence,  $\partial\chi/\partial p_c < 0$ , of the magnetic susceptibility while  $\partial\chi/\partial p_{a^*} > 0$ . This observation suggests that antiferromagnetic exchange interactions are strengthened by uniaxial pressure along the  $c$  axis and weakened upon application of  $p \parallel a^*$ . Notably, however, the long-range magnetic ordering temperatures do not follow this trend as  $\partial T_N/\partial p_c < 0$ , which further highlights the complex nature of magnetism in  $\text{Gd}_2\text{PdSi}_3$ .

## V. CONCLUSIONS

High-resolution dilatometry was used to study the interplay between magnetism and the lattice of single crystalline  $\text{Gd}_2\text{PdSi}_3$ . Strong magnetoelastic coupling and field effects up to high temperatures are found. Pronounced anomalies in the thermal expansion, magnetostriction, and magnetization allow us to obtain the magnetic phase diagram. This yields in particular several phases and previously unreported phase boundaries for  $B \parallel c$  whereas the B vs T phase diagram for  $B \parallel a^*$  has not yet been reported at all in the literature. Grüneisen analysis shows the onset of magnetic contributions well above  $T_{N1}$ , and the pressure dependencies of ordering phenomena are obtained. In particular, we find that uniaxial pressure strongly enhances the skyrmion lattice phase.

## ACKNOWLEDGMENTS

We thank I. Mazilu and Y. Xu for support in the crystal growth. We acknowledge financial support by BMBF via the project SpinFun (Grant No. 13XP5088) and by the Deutsche Forschungsgemeinschaft (DFG) under Germany's Excellence Strategy, Grant No. EXC2181/1-390900948 (the Heidelberg STRUCTURES Excellence Cluster), through Project No. KL 1824/13-1, and within the SFB 463.

- [1] R.-D. Hoffmann and R. Pöttgen, *Z. Kristallogr. - Cryst. Mater.* **216**, 127 (2001).
- [2] Z.-Y. Pan, C.-D. Cao, X.-J. Bai, R.-B. Song, J.-B. Zheng, and L.-B. Duan, *Chin. Phys. B* **22**, 056102 (2013).
- [3] S. Majumdar and E. V. Sampathkumaran, *Phys. Rev. B* **63**, 172407 (2001).
- [4] S. Majumdar, E. V. Sampathkumaran, P. L. Paulose, H. Bitterlich, W. Löser, and G. Behr, *Phys. Rev. B* **62**, 14207 (2000).
- [5] S. Majumdar, H. Bitterlich, G. Behr, Löser, P. L. Paulose, and E. V. Sampathkumaran, *Phys. Rev. B* **64**, 012418 (2001).
- [6] P. L. Paulose, E. V. Sampathkumaran, H. Bitterlich, G. Behr, and W. Löser, *Phys. Rev. B* **67**, 212401 (2003).
- [7] C. D. Cao, R. Klingeler, H. Vinzelberg, N. Leps, W. Löser, G. Behr, F. Muranyi, V. Kataev, and B. Büchner, *Phys. Rev. B* **82**, 134446 (2010).
- [8] T. Kurumaji, T. Nakajima, M. Hirschberger, A. Kikkawa, Y. Yamasaki, H. Sagayama, H. Nakao, Y. Taguchi, T. Arima, and Y. Tokura, *Science* **365**, 914 (2019).



- [9] M. Hirschberger, T. Nakajima, M. Kriener, T. Kurumaji, L. Spitz, S. Gao, A. Kikkawa, Y. Yamasaki, H. Sagayama, H. Nakao *et al.*, *Phys. Rev. B* **101**, 220401(R) (2020).
- [10] S. Majumdar, M. Mahesh Kumar, R. Mallik, and E. Sampathkumaran, *Solid State Commun.* **110**, 509 (1999).
- [11] S. R. Saha, H. Sugawara, T. D. Matsuda, Y. Aoki, H. Sato, and E. V. Sampathkumaran, *Phys. Rev. B* **62**, 425 (2000).
- [12] S. Majumdar, E. V. Sampathkumaran, S. Berger, M. Della Mea, H. Michor, E. Bauer, M. Brando, J. Hemberger, and A. Loidl, *Solid State Commun.* **121**, 665 (2002).
- [13] D. Kaczorowski and H. Noel, *J. Phys.: Condens. Matter* **5**, 9185 (1993).
- [14] C. Tien, L. Luo, and J. S. Hwang, *Phys. Rev. B* **56**, 11710 (1997).
- [15] D. X. Li, A. Dönni, Y. Kimura, Y. Shiokawa, Y. Homma, Y. Haga, E. Yamamoto, T. Honma, and Y. Onuki, *J. Phys.: Condens. Matter* **11**, 8263 (1999).
- [16] D. X. Li, S. Nimori, Y. Shiokawa, Y. Haga, E. Yamamoto, and Y. Onuki, *Phys. Rev. B* **68**, 012413 (2003).
- [17] S. R. Saha, H. Sugawara, T. D. Matsuda, H. Sato, R. Mallik, and E. V. Sampathkumaran, *Phys. Rev. B* **60**, 12162 (1999).
- [18] M. Hirschberger, L. Spitz, T. Nomoto, T. Kurumaji, S. Gao, J. Masell, T. Nakajima, A. Kikkawa, Y. Yamasaki, H. Sagayama *et al.*, *Phys. Rev. Lett.* **125**, 076602 (2020).
- [19] A. Szytuła, M. Hofmann, B. Penc, M. Ślaski, S. Majumdar, E. V. Sampathkumaran, and A. Zygmunt, *J. Magn. Magn. Mater.* **202**, 365 (1999).
- [20] F. Tang, M. Frontzek, J. Dshemuchadse, T. Leisegang, M. Zschornak, R. Mietrach, J.-U. Hoffmann, W. Löser, S. Gemming, D. C. Meyer *et al.*, *Phys. Rev. B* **84**, 104105 (2011).
- [21] F. Tang, P. Link, M. Frontzek, A. Schneidewind, W. Löser, and M. Loewenhaupt, *J. Phys.: Conf. Ser.* **251**, 012004 (2010).
- [22] M. Frontzek, Ph.D. thesis, Technische Universität Dresden, 2009, <https://nbn-resolving.org/urn:nbn:de:bsz:14-qucosa-24779>.
- [23] M. Smidman, C. Ritter, D. T. Adroja, S. Rayaprol, T. Basu, E. V. Sampathkumaran, and A. D. Hillier, *Phys. Rev. B* **100**, 134423 (2019).
- [24] K. Mukherjee, T. Basu, K. K. Iyer, and E. V. Sampathkumaran, *Phys. Rev. B* **84**, 184415 (2011).
- [25] H. Zhang, Q. Huang, L. Hao, J. Yang, K. Noordhoek, S. Pandey, H. Zhou, and J. Liu, *New J. Phys.* **22**, 083056 (2020).
- [26] Here,  $\Delta a = a(300\text{ K}) - a(2\text{ K})$  and  $\Delta c$  analogously.
- [27] I. Mazilu, Ph.D. thesis, Technische Universität Darmstadt, 2006.
- [28] Y. Xu, M. Frontzek, I. Mazilu, W. Löser, G. Behr, B. Büchner, and L. Liu, *J. Cryst. Growth* **318**, 942 (2011).
- [29] D. S. Inosov, D. V. Evtushinsky, A. Koitzsch, V. B. Zabolotnyy, S. V. Borisenko, A. A. Kordyuk, M. Frontzek, M. Loewenhaupt, W. Löser, I. Mazilu *et al.*, *Phys. Rev. Lett.* **102**, 046401 (2009).
- [30] R. Küchler, T. Bauer, M. Brando, and F. Steglich, *Rev. Sci. Instrum.* **83**, 095102 (2012).
- [31] J. Werner, W. Hergett, M. Gertig, J. Park, C. Koo, and R. Klingeler, *Phys. Rev. B* **95**, 214414 (2017).
- [32] C. Cao, C. G. F. Blum, T. Ritschel, S. Rodan, L. Giebeler, D. Bombor, S. Wurmehl, and W. Löser, *CrystEngComm* **15**, 9052 (2013).
- [33] A. Tari, *The Specific Heat of Matter at Low Temperatures* (Published by Imperial College and distributed by World Scientific, Singapore 2003).
- [34] See Supplemental Material at <http://link.aps.org/supplemental/10.1103/PhysRevB.103.184424> for additional figures and tables.
- [35] P. Gegenwart, *Rep. Prog. Phys.* **79**, 114502 (2016).
- [36] R. Klingeler, J. Geck, S. Arumugam, N. Tristan, P. Reutler, B. Büchner, L. Pinsard-Gaudart, and A. Revcolevschi, *Phys. Rev. B* **73**, 214432 (2006).
- [37] The  $T$  scale for  $\alpha_{c,\text{mag}}$  was shifted by +0.4 K to match the specific heat anomaly.
- [38] V. M. Kalita, A. F. Lozenko, and S. M. Ryabchenko, *Low Temp. Phys.* **26**, 489 (2000).
- [39] V. M. Kalita, A. F. Lozenko, and P. A. Trotsenko, *Low Temp. Phys.* **28**, 263 (2002).
- [40] K. Dey, S. Sauerland, B. Ouladdiaf, K. Beauvois, H. Wadepohl, and R. Klingeler, *Phys. Rev. B* **103**, 134438 (2021).
- [41] For the field-cooled warming protocol, the sample is cooled in the applied field to the lowest temperatures and measured during the subsequent warming process.
- [42] Magnetization measurements have been performed following the zero-field cooling protocol unless stated otherwise; i.e., the sample was cooled to the lowest temperatures before the field was applied and the data were recorded during warming.
- [43] M. Hirschberger, T. Nakajima, S. Gao, L. Peng, A. Kikkawa, T. Kurumaji, M. Kriener, Y. Yamasaki, H. Sagayama, H. Nakao *et al.*, *Nat. Commun.* **10**, 5831 (2019).
- [44] T. H. K. Barron and G. K. White, *Heat Capacity and Thermal Expansion at Low Temperatures*, The International Cryogenic Monograph Series (Kluwer Academic, Dordrecht/Plenum, New York, 1999).
- [45] R. Klingeler, B. Büchner, S.-W. Cheong, and M. Hücker, *Phys. Rev. B* **72**, 104424 (2005).
- [46] A. Bauer, M. Garst, and C. Pfleiderer, *Phys. Rev. Lett.* **110**, 177207 (2013).
- [47] I. Levatić, P. Popčević, V. Šurija, A. Kruchkov, H. Berger, A. Magrez, J. S. White, H. M. Rønnow, and I. Živković, *Sci. Rep.* **6**, 21347 (2016).
- [48] A. Chacon, A. Bauer, T. Adams, F. Rucker, G. Brandl, R. Georgii, M. Garst, and C. Pfleiderer, *Phys. Rev. Lett.* **115**, 267202 (2015).
- [49] Y. Nii, T. Nakajima, A. Kikkawa, Y. Yamasaki, K. Ohishi, J. Suzuki, Y. Taguchi, T. Arima, Y. Tokura, and Y. Iwasa, *Nat. Commun.* **6**, 8539 (2015).
- [50] For MnSi, this also holds for pressure along [111] and [110]. From our data, only uniaxial pressure effects  $p \parallel c$  are accessible, so a comparison for the other directions cannot be made.
- [51] S. Hayami, S.-Z. Lin, and C. D. Batista, *Phys. Rev. B* **93**, 184413 (2016).
- [52] R. Mallik, E. V. Sampathkumaran, M. Strecker, and G. Wortmann, *Europhys. Lett.* **41**, 315 (1998).
- [53] Z. Wang, K. Barros, G.-W. Chern, D. L. Maslov, and C. D. Batista, *Phys. Rev. Lett.* **117**, 206601 (2016).
- [54] N. Johannsen, A. Vasiliev, A. Oosawa, H. Tanaka, and T. Lorenz, *Phys. Rev. Lett.* **95**, 017205 (2005).